Article:

Jiang, J., Sun, Z., Duan, F. et al. (7 more authors) (2018) Disguised bionic sonar signal waveform design with its possible camouflage application strategy for underwater sensor platforms. IEEE Sensors Journal, 18 (20). pp. 8436-8449. ISSN 1530-437X

https://doi.org/10.1109/JSEN.2018.2865730

Disguised Bionic Sonar Signal Waveform Design with Its Possible Camouflage Application Strategy for Underwater Sensor Platforms

Jiajia Jiang, *IEEE Member*, Zhongbo Sun, Fajie Duan, Wei Liu, *IEEE Senior Member*, Xianquan Wang, Chunyue Li, Lingran Bu, Xiao Fu, Tingting Huang and Ling Ma

***Abstract*— The covertness of an active sonar is a very important issue and the sonar signal waveform design problem is studied to improve covertness of the system. Many marine mammals produce call pulses for communication and echolocation, and existing interception systems normally classify these biological signals as ocean noise and filter them out. Based on this, a disguised sonar signal waveform design approach with its camouflage application strategy for underwater sensor platforms is proposed by utilizing bio-inspired steganography. We first construct bionic sonar signal waveforms which are very close to the true whale whistle, and then embed these constructed bionic sonar signal waveforms into the true whale call trains to hide the real sonar signal waveforms. According to the time-frequency (TF) structure of the true whale whistle, a bionic sonar signal model is established to generate the proposed sonar signal waveforms. A single sonar signal is used to measure the range of the target and a combination of two sonar signals is utilized for measuring its speed. A high-performance range and speed measurement algorithm is deduced in detail. Based on the constructed signal waveforms and the characteristics of false killer whale call trains, a camouflage application strategy is designed to improve the camouflage ability of the sonar signal sequence. Finally, simulation results are provided to verify the performance of the proposed method.**

***Index Terms*—Covert sonar; sonar waveform design; bionic sonar; disguised sonar waveform design.**

I. Introduction

By sending out signals for target detection, an active sonar system unavoidably risks being detected and identified by the others, too. In the last few decades, many methods have been proposed to improve the stealth capability of active sonar systems through signal waveform design [1-12].

Some methods try to constantly change the parameters of the transmitted signals to increase of the identification difficulty, such as period-hopping [2], frequency-hopping [3-4], time-hopping [5] and so on. Although they can improve the covertness of signals, there is still much further work to be done since those changed-parameters signals have some distinct features. For example, for frequency-hopping signals, each pulse could be continuous-wave (CW) or linear frequency modulated (LFM); however, the CW pulses have the feature of being of rectangle in the time domain and single frequency in the frequency domain, while LFM pulses are of both rectangle in the time domain and linearly changed frequency in the frequency domain [6]. As a result, these signals can be identified and classified easily in practice [11-12].

Some other methods use low signal noise ratio (SNR) signals with LFM [6], FM-CW [7-8], or other stealth signals, such as pseudorandom [9-10] or chaotic codes [10] to increase the difficulty of being detected. Achieving a high degree of covertness, these signals can still be detected by some methods, such as envelope detection, energy detection and energy spectral density analysis methods, etc. [13-14]. Besides, a sonar system using the low SNR signals requires a long-time energy accumulation process for target detection, which severely affects the detection efficiency.

Due to the similarity of considered problems, many ideas in radar signal waveform design [15-17] can also be employed here, and for the specific covert signal waveform design problem, those ideas in radar also fall into the above two categories [4, 9].

Another direction for sonar waveform design is the nature-inspired approach. Given nature's ability to address complex, large-scale problems with robust, adaptable, and efficient solutions resulting from many years of evolution, researchers look to natural systems for inspiration and methods to solve problems in human-created artificial environments. Based on the bio-sonar systems in nature, Rolf Muller *et al.* presented a detailed review and discussion about bio-inspired engineering, and pointed out that bioinspired engineering could capitalize on some of its strengths to serve as a model system for basic automation methodologies for the bioinspired engineering process in future research [18]. In [19], Chris Capus *et al.* designed a novel and interesting bio-inspired wideband sonar signal waveform based on the double down-chirp structure of clicks of bottlenose dolphin, evaluated its performance and obtained excellent results. In [20], inspired by the vocalization of humpback whales and dolphins, Timothy Leighton and Paul White proposed a possible sonar scheme for targets detection in bubble clouds, and a possible radar scheme

Manuscript received xx xx, 20xx. This work was supported in part by the TianJin Natural Science Foundations of China under Grant No. 17JCQNJC01100, National Natural Science Foundations of China under Grant No. 61501319, 51775377, National key research and development plan (2017YFF0204800), Young Elite Scientists Sponsorship Program By Cast of China under Grant No. 2016QNRC001.

Jiajia Jiang, Zhongbo Sun, Fajie Duan, Xianquan Wang, Lingran Bu, Chunyue Li, Xiao Fu, Tingting Huang and Ling Ma are with the State Key Lab of Precision Measuring Technology and Instruments, Tianjin, 300072, China. (Corresponding author: Zhongbo Sun (zbsun@tju.edu.cn)).

Wei Liu is with the Department of Electronic and Electrical Engineering, University of Sheffield, UK.

for the detection of buried explosives and catastrophe victims. And the relevant experimental results showed the validity of their schemes. In [21], by using the idea of camouflage similar to this paper, a bio-inspired steganography for secure underwater acoustic communications was proposed by us based on the sperm whale calls and about 37.5bit/s communication rate is completed through lake experiments. In [22], inspired by what little is known about dolphin echolocation receiving mechanisms, Peter Dobbins proposed a very interesting and new concept for a sonar receiver based on a pair of endfire array model from dolphin' teeth, and showed that endfire array beam patterns had minimal near-field degradation and a pair of endfire arrays could be used in a monopulse mode for angular localization. These results are very enlightening to us. In [23], Rolf Müller *et al.* compared beamwidth in biosonar and engineered sonar with each other and to the theoretical beamwidth limit for the respective ratio of sonar aperture size and wave-length and obtaind some very interesting and instructive results. In [24], Michele Vespe *et al.* introduced a range of strategies employed by bats and considered how these might be exploitable in future radar systems. These bio-inspired ideas and in-depth analysis are very interesting and inspirational. However, to our best knowledge, the covertness issue has not been considered yet in this context.

As can be seen in [25-27], present interception systems almost always classify biological signals as ocean noise and try to filter them out. Based on this, we propose a covert sonar signal waveform design approach with its possible camouflage application strategy by utilizing bio-inspired steganography. By analyzing the time-frequency (TF) structures of whistles emitted by false killer whales, it is found that the TF structures of hyperbolic frequency modulated (HFM) signals are very similar to those of false killer whales. Therefore, based on the HFM signal model, a bionic sonar signal model is presented, which is then utilized to construct disguised and bionic sonar signal waveforms to accomplish disguised and covert active sonar detection tasks. The main contributions of this paper can be summarized as follows:

(1) Different from conventional parameter-changing or low SNR sonar signal waveforms, a new type of disguised, and bionic sonar signal waveform design is proposed;

(2) According to the TF characteristics of false killer whale calls, an imitation sonar signal mode is presented, with a very good match to the true whistle of false killer whales.

(3) A computationally efficient target range and speed measurement algorithm employing the characteristics of time resolution and Doppler tolerance of the constructed bionic sonar signal waveforms is developed.

(4) The proposed approach overcomes the trade-off between long-range detection and covertness. It can obtain covertness camouflage even if the SNR of the transmitted signals is very high. On the other hand, it can improve the covertness by reducing the SNR for a short range target detection task.

II. Analysis and Preprocessing of False Killer Whale Calls

A. Characteristics of false killer whale calls

When navigating, communicating, hunting, and avoiding predators in dark or limited vision waters, false killer whales produce clicks and whistles [28-30], as shown in Fig. 1.

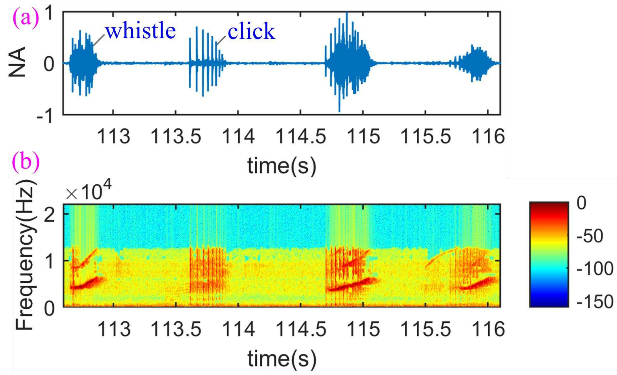

Fig. 1. Clicks and whistles produced by the false killer whale.

The clicks are produced in series, quite variable in structure and have frequency peaks from 20 kHz to 120 kHz [28-29]. Whistles are characterized by a continuous waveform, which appears on a TF spectrogram as a single tone with little or no harmonic or side-band structure. The frequency of whistles ranges from about 4 kHz to 10 kHz [30]. Whistles, with relative long-time duration, are believed to serve as some sort of communication or social cohesion roles. The frequency distribution of whistles is close to the frequency distribution of mid-frequency sonar signals, which is beneficial for remote target detection.

B. Preprocessing and statistical analysis of false killer whale calls

The original high quality call of 7 minutes and 25 seconds, produced by a false killer whale, was recorded with a 44.1ksps sampling rate. Unavoidably, the signal was polluted by the Gaussian ocean ambient noise [31], and as can be seen from the TF spectrograms in Figs. 1 and 2, the whistles of false killer whales are short-time stationary. In such a case, a Wiener filter [32] can be utilized to remove the background noise of the recorded signal. The Wiener filter is based on a priori SNR estimation; the first 0.25 seconds of the original call train is utilized to model the noise, and then the original call train is transformed into the short-time Fourier transform (STFT) domain by using a 60% overlapping Hamming window with a N=1102 samples length (25 ms). The time-domain waveforms of partial original and denoised false killer whale call trains are shown in Fig. 2(a), and their TF spectrograms are shown in Fig. 2(b) and 2(c), respectively. Comparing Fig. 2(a), 2(b) and 2(c), it can be seen that the ocean ambient noise has been filtered out effectively.

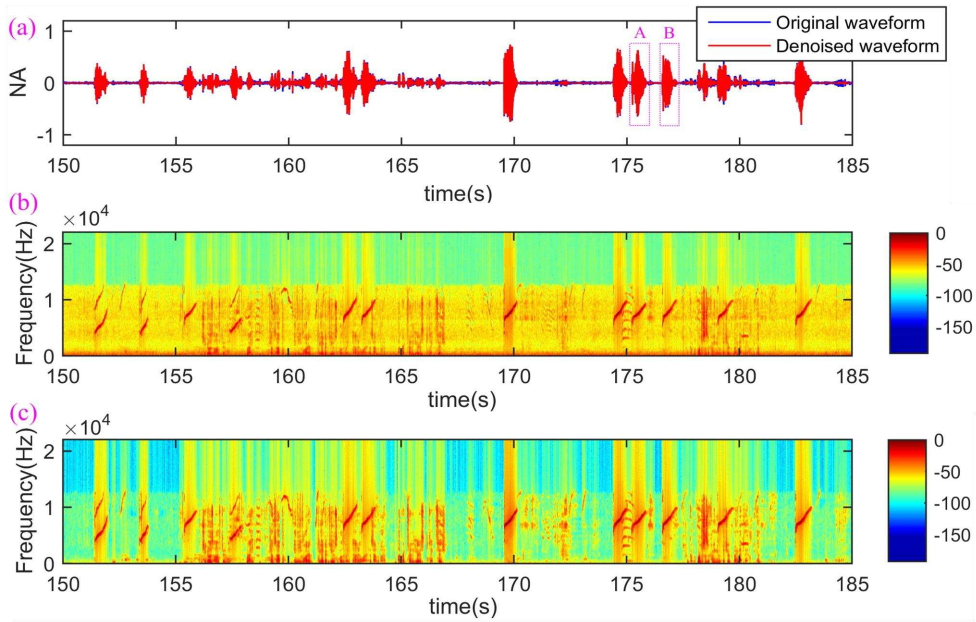

Fig. 2. (a) Part of the original and denoised false killer whale call trains with normalized amplitude (NA); (b) TF spectrogram of the original false killer whale call train; (c) TF spectrogram of the denoised false killer whale call train.

Table 1. Six types of whistles

Type	Description	Number
Type-1	Hyperbolic-like up-sweep	80
Type-2	Hyperbolic-like double up-sweep	15
Type-3	Parabolic-like up-sweep	6
Type-4	Parabolic-like down-sweep	4
Type-5	Sine-like	5
Type-6	Harmonic-like down-sweep	4

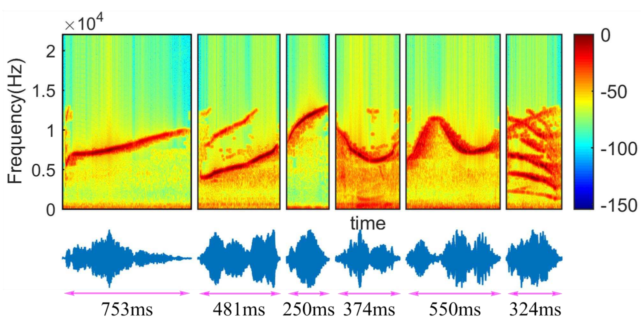

Fig. 3. Six types of TF spectrogram and waveform representations.

To analyze the TF characteristics of every whistle of false killer whales, the endpoint detection technique in [33] based on the short-time energy is used to collect all whistles from the denoised call train, and 114 whistles are obtained in total. Then, by comparing the shapes of the TF spectrograms of whistles, the TF spectrograms of 114 whistles are classified into six distinct types artificially, as shown in Table 1 and Fig. 3.

As can be seen in Table 1, the Type-1 whistles constitute about 70% of all whistles. This indicates that it is more representative to construct the bionic and disguised sonar signal waveforms by imitating the Type-1 whistles.

In addition, as seen from Fig. 3, the TF shape of Type-1 whistles is very similar to that of the HFM signal waveforms. Therefore, in the next section, we propose a bionic sonar signal model based on the HFM model.

III. Bionic Sonar Signal Model

A HFM signal with a duration T can be written as [34]

$$\overline{s}_s(t) = A(t)\exp\left[j2\pi\left(\frac{1}{b}\ln\left(1+bf_L t\right)\right)\right] \quad 0 \le t \le T \qquad (1)$$

where $b = (f_L - f_H)/(f_L f_H T)$ defines a unique sweep factor and $A(t)$ denotes the signal envelope. The instantaneous frequency is defined as

$$\overline{f}_s(t) = \frac{\partial}{\partial t}\left[\frac{1}{b}\ln\left(1+bf_L t\right)\right] = \frac{f_L}{1+bf_L t} \qquad (2)$$

Obviously, $\overline{f}_s(t)$ is a hyperbolic function of time t. The start frequency $\overline{f}_s(0)$ and the end frequency $\overline{f}_s(T)$ are f_L and f_H, respectively. Clearly, the curvature of the HFM signal waveform only depends on its frequency range and duration.

However, when trying to fit the TF shape of the Type-1 whistle using the HFM signal waveform, we find that there exists a clear mismatch between them, as shown in Fig. 4. This mismatch is caused by the different curvatures between the Type-1 whistle and the HFM signal waveform. However, once the frequency range and the duration of an HFM signal waveform are fixed, its curvature cannot be changed any more.

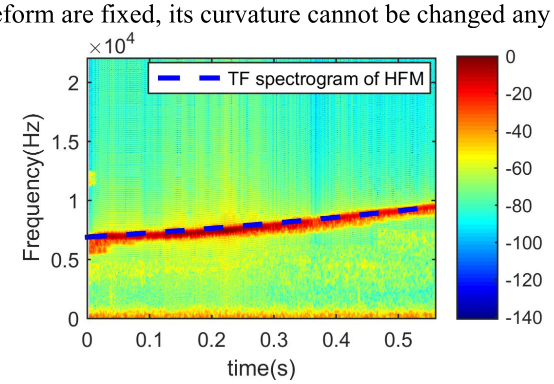

Fig. 4. TF spectrograms of Type-1 whistle and HFM.

To have a close match to the true whistle, based on the HFM signal model, a novel bionic sonar signal model is proposed as follows

$$s_s(t) = A(t)\exp\left[j2\pi\left(\frac{1}{b}\ln\left(1+bf_L t\right)+f_c t\right)\right] \quad 0 \le t \le T \quad (3)$$

where f_c plays the part of the carrier frequency. The instantaneous frequency is defined as

$$f_s(t) = \frac{\partial}{\partial t}\left[\frac{1}{b}\ln\left(1+bf_L t\right)+f_c t\right] = \frac{f_L}{1+bf_L t}+f_c \quad (4)$$

which continuously and monotonically goes from the start frequency $f_s(0) = f_L + f_c$ to the end frequency $f_s(T) = f_H + f_c$ within a pulse duration in a hyperbolic way. The proposed bionic sonar signal model is equivalent to the HFM signal model when $f_c = 0$ and therefore more general. Most importantly, due to the introduction of $f_c t$ in (3), the curvature of the TF spectrogram of $s_s(t)$ now depends on its frequency range, duration and the parameter f_c. When the frequency range and the duration of $s_s(t)$ are fixed, its curvature can be adjusted by changing f_c, which is very important for us to imitate the TF shape of the true whistle as closely as possible.

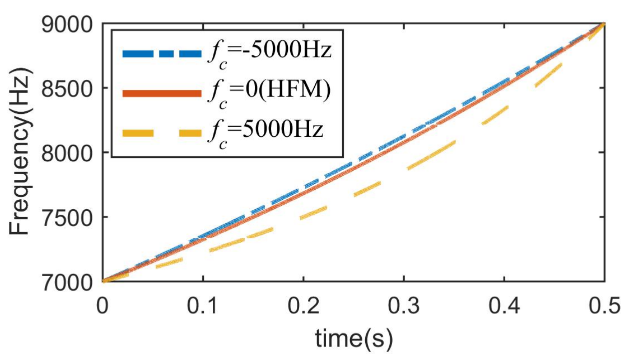

Fig. 5. TF spectrograms of $s_s(t)$.

For example, the instantaneous frequency curves of $s_s(t)$ with three different f_c parameters, the frequency range from 7000 to 9000 Hz and the duration $T = 500ms$, are shown in Fig. 5. It can be seen that with the change of f_c, the curvature of the TF spectrogram of $s_s(t)$ changes constantly. Therefore, one can imitate and match the TF shape of the true whistle as closely as possible by adjusting f_c on the condition that the frequency range and the duration are fixed.

So far the signal envelope $A(t)$ has not been considered yet. It can be seen from Figs. 2 and 3 that different from the conventional sonar signal waveforms (e.g. CW, LFM, HFM), the whistle envelopes are not rectangular, and varied with different irregularity for different whistles. In order to fit the envelopes of the whale whistles, an envelope extraction method based on STFT is presented next.

Firstly, the STFT of the denoised whistles is calculated. The discrete-time signal $x(n)$ of the denoised whistle can be defined as

$$x(n) = a(n)\cos\left[\phi(n)\right] \quad (5)$$

where $a(n)$ and $\phi(n)$ are the envelope and phase of $x(n)$. The STFT of $x(n)$ is defined as

$$X(\tau,\omega) = \sum_{n=-\infty}^{\infty} x(n)w(n-\tau)\exp(-j\omega n) \quad (6)$$

where $w(n)$ is a Hamming window with a *N*-sample length. This definition can be understood and visualized by cutting $x(n)$ into small segments with the window function in the time domain, and $x(n)$ is expected to be relatively constant in amplitude and frequency over *N* samples. These segments are indexed with *m,* and $x(n)$ is assumed to have *M* such segments. $X_m(\omega)$ is the discrete Fourier transform (DFT) for the *m*-th segment, and the extracted envelope $a_r(n)$ of $x(n)$ is obtained from $X_m(\omega)$.

Secondly, the start time point of the *m*-th segment is indexed by τ_m, the amplitude of $x(n)$ at τ_m is $a(\tau_m) = A_m$, and the peak value of $X_m(\omega)$ is $A_{mp} = \max\left|X_m(\omega)\right|$. Since A_{mp} is modulated by the Hamming window and DFT, an amplitude recovery factor K_r is required to restore the amplitude of the segment. The Hamming window is defined as [35]

$$w[n] = \lambda - (1-\lambda)\cos\left[2\pi n / N\right] \quad n = 0,1,...,N \quad (7)$$

with $\lambda = 0.54$. The DFT of $w[n]$ is

$$W(\omega) = \lambda D(\omega) + \frac{1-\lambda}{2}\left[D\left(\omega - \frac{2\pi}{N}\right) + D\left(\omega + \frac{2\pi}{N}\right)\right] \quad (8)$$

where

$$D(\omega) = \exp(j\omega/2)\cdot\sin(N\omega/2)\sin(\omega/2) \quad (9)$$

The amplitude spectrum of the Hamming window is

$$W_a(\omega) = \left|W(\omega)\right|$$
$$= \lambda\frac{\sin\left(\frac{N}{2}\omega\right)}{\sin\left(\frac{\omega}{2}\right)} + \frac{1-\lambda}{2}\left[\frac{\sin\left(\frac{N}{2}\omega+\pi\right)}{\sin\left(\frac{\omega}{2}+\frac{\pi}{N}\right)} + \frac{\sin\left(\frac{N}{2}\omega-\pi\right)}{\sin\left(\frac{\omega}{2}-\frac{\pi}{N}\right)}\right] \quad (10)$$

Using the L′Hospital rule, the amplitude of the Hamming window at $\omega = 0$ is given by

$$W_a(0) = N\lambda \quad (11)$$

Since the amplitude spectrum obtained from DFT will be scaled by the factor N, it is necessary to multiply the result with $1/N$ to eliminate the coefficient N in equation (11). Then, the amplitude correction factor of the Hamming window is

$$K_H = 1/\lambda \quad (12)$$

The amplitude correction factor of the DFT is

$$K_D = 2/N \tag{13}$$

Then one can obtain the amplitude recovery factor K_r as

$$K_r = K_H K_D = 2/\lambda N \tag{14}$$

Finally, let $a_r(\tau_m) = K_r A_{mp}$ and the amplitude of $a_r(\tau_m)$ is restored to the same level as the whale whistle envelope. Using the piecewise cubic Hermit interpolation to add the remaining points of $a_r(n)$, the extracted envelope of $x(n)$ is obtained.

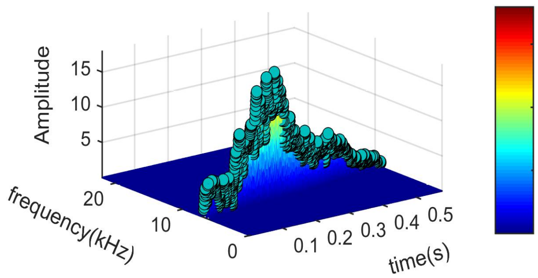

Fig. 6. TF diagram of the Type-1 whale whistle.

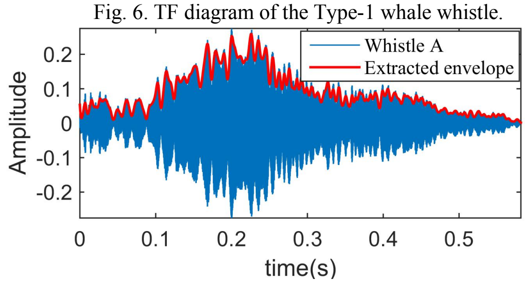

Fig. 7. Waveform of the Type-1 whale whistle and the corresponding extracted envelope.

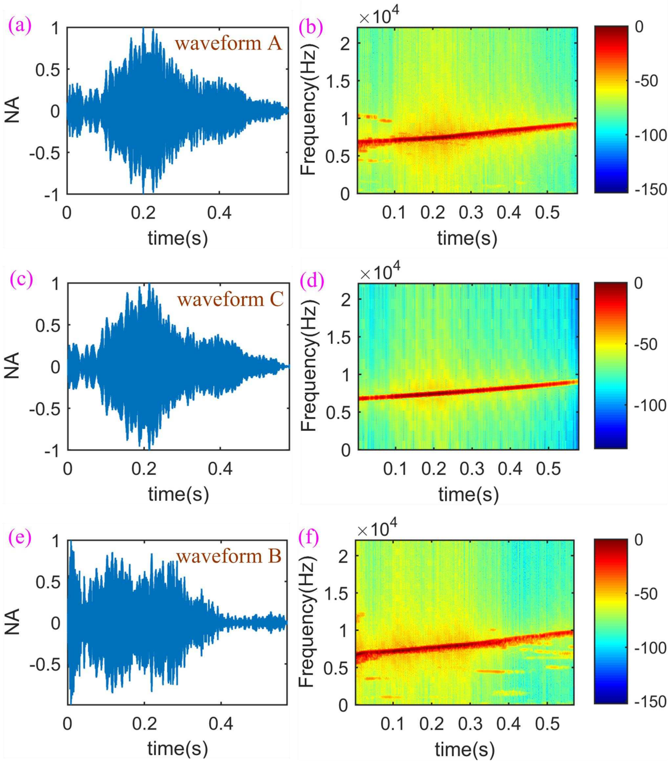

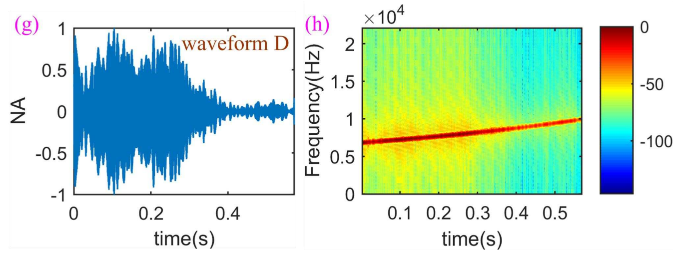

Fig. 8. (a) The false killer whistle A, (b) the TF spectrogram of the false killer whistle A, (c) the constructed bionic sonar signal waveform C, (d) the TF spectrogram of the constructed bionic sonar signal waveform, (e) the false killer whistle B, (f) the TF spectrogram of the false killer whistle B, (g) the constructed bionic sonar signal waveform D, (h) the TF spectrogram of the constructed bionic sonar signal waveform.

The type-1 false killer whistle (see Fig. 2(a)) was selected to verify the effectiveness of the envelope extraction method described above. As shown in Fig. 6, the ridge of the three-dimensional (3-D) time-frequency diagram of $a_r(\tau_m)$ basically coincides with the points of $a_r(\tau_m)$, and the points of $a_r(\tau_m)$ are sparser. After interpolation, the extracted envelope $a_r(n)$ and the waveform of the whale whistle are shown in Fig. 7, where it can be seen that $a_r(n)$ matches the envelope of the whale whistle well.

Based on the bionic sonar signal model proposed above, the construction of 80 bionic sonar signal waveforms corresponding to 80 Type-1 whale whistles listed in Table 1 is achieved. For visualization, we choose two representative false killer whistles A and B (please see the two whistles in Fig. 2 (a)) to serve as the reference waveforms to be matched and imitated. The true whistles and their TF spectrograms and the constructed bionic sonar signal waveforms C and D and their TF spectrograms are shown in Fig. 8. It can be seen that the constructed bionic sonar signal waveforms can highly match the true whale whistles in terms of not only envelopes but also TF spectrograms.

IV. Time Resolution, Doppler Tolerance and Cross-correlation of the Constructed Bionic Sonar Signal Waveforms

Time resolution (corresponding to range resolution) and Doppler tolerance (related to Doppler resolution) are two key indicators for radar and sonar signal waveform design [24].

For sonar applications, when $B \le 0.1 f_0$, the signal is considered to be narrowband [36], where B is the bandwidth and f_0 is the center frequency of the signal. Based on this criterion, it can be verified that all of the 80 constructed bionic sonar signal waveforms are wideband. Therefore, the wideband ambiguity function (WAF) is used to examine the time resolution and Doppler tolerance [37].

$$WAF_s(\alpha,\tau) = \sqrt{\alpha}\int s(t)\, s^*\big(\alpha(t-\tau)\big)dt \tag{15}$$

where $\alpha = (c-v)/(c+v) \approx 1 - 2v/c$ is the Doppler scale factor, $\tau = 2R/c$ is the propagation time delay, R is the target range (or distance), '*' is the complex conjugate operator, v is the relative speed between the sonar system and the target, and

c is the sound speed in water.

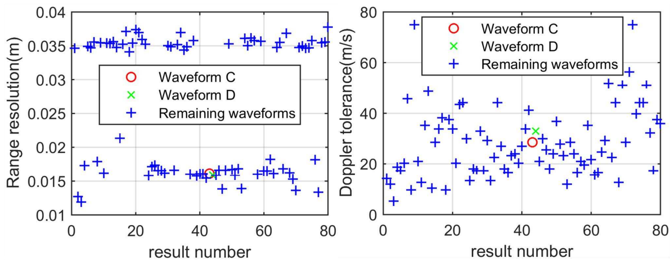

Fig. 9. Range resolution and Doppler tolerance of the 80 constructed bionic sonar signal waveforms.

The range resolution (corresponding to the time resolution) and speed tolerance (corresponding to the Doppler tolerance) of the 80 constructed bionic sonar signal waveforms are computed and the results are shown in Fig. 9.

It can be seen that all the constructed bionic sonar signal waveforms have excellent range resolution and speed tolerance; however, their WAF has certain coupling in the time-Doppler plane. For visualization, the WAF of the constructed bionic sonar signal waveform C corresponding to whistle A in Fig. 8(a) is provided in Fig. 10.

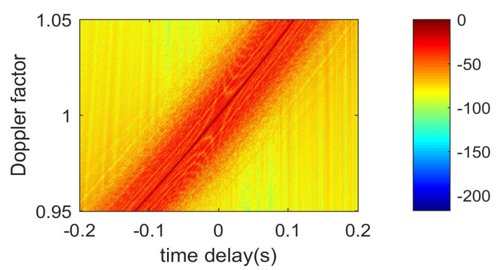

Fig. 10. WAF diagram of the sonar signal C.

It is well-known that a good time resolution means that a sonar signal waveform can be used for high-accuracy range measurement of targets, while a good Doppler resolution allows high-accuracy speed measurement of targets. On the contrary, a good Doppler tolerance means that the sonar signal waveform is insensitive to the relative movement between the sonar system and the target, and therefore a low speed resolution. Based on the above analysis and results, one can know that a single constructed bionic sonar signal waveform can be used for achieving high range resolution and resolving multiple closely located targets, but cannot be used for high speed resolution. In order to solve this speed measurement issue, a speed estimation method through a combination of two constructed bionic sonar signal waveforms with low cross-correlation between them is proposed next.

The 80 constructed bionic sonar signal waveforms can be used to form $C_{80}^{2}=3160$ combinations. Then, the cross-correlation between two constructed bionic sonar signal waveforms in each combination is calculated. With a threshold value of 0.4 for the cross-correlation, 326 combinations are obtained, and therefore can be used to measure the speed of targets using the following method.

V. Speed and Range Estimation

A. Effect of Doppler on sonar signal waveforms

Before presenting the range and speed estimation methods, we first review the effect of Doppler on sonar signal waveforms.

When a transmitted sonar signal arrives at a moving target with a constant speed, it is reflected back by the target, and the return echo signal will be Doppler-distorted, which means the duration of the return echo signal will be compressed or stretched, and its frequency range will be shifted [24, 38]. Suppose that the relative speed between the sonar system and the target is v (where $v>0$ for moving away from the target and $v<0$ for moving towards the target), and the initial range of the target is R, the return echo signal from the target can be expressed as

$$s_r(t)=\sqrt{\alpha}s_s(\alpha t)$$
$$=\sqrt{\alpha}A(\alpha t)\exp\left\{j2\pi\left[\frac{1}{b}\ln\left(1+\alpha bf_L t\right)+\alpha f_c t\right]\right\}0\le t\le T/\alpha \tag{16}$$

Ignoring noise and propagation loss, the instantaneous frequency of $s_r(t)$ is written as

$$f_r(t)=\frac{\partial}{\partial t}\left[\frac{1}{b}\ln\left(1+\alpha bf_L t\right)+\alpha f_c t\right]=\frac{\alpha f_L}{1+\alpha bf_L t}+\alpha f_c \tag{17}$$

We define two new parameters Δf and Δt as

$$\Delta f=\left(\alpha-1\right)f_c=-2vf_c/\left(c+v\right) \tag{18}$$

$$\Delta t=(1-\alpha)/(\alpha bf_L)=2vf_H T/(c-v)(f_H-f_L) \tag{19}$$

Combining (4) and (17)-(19), the following relationship can be obtained

$$f_r\left(t\right)=f_s(t+\Delta t)+\Delta f \tag{20}$$

Equation (20) indicates that the instantaneous frequency of the return echo signal $s_r\left(t\right)$ can be obtained through shifts in time and frequency axis of the transmitted sonar signal $s_s\left(t\right)$, as shown in Fig. 11.

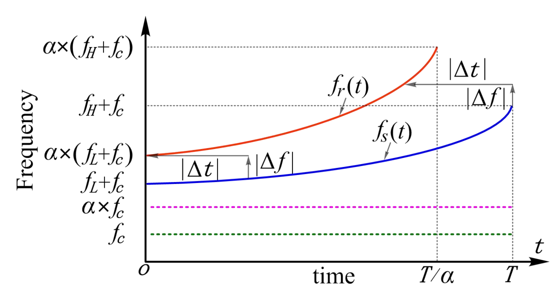

Fig. 11. Time delay and frequency shift of the sonar signal waveform.

However, since the duration of signal is changed by the compression or stretching caused by the Doppler effect, there is a partial overlap between the TF spectrogram of $s_r\left(t\right)$ and that of the shifted $s_s\left(t\right)$ in time and frequency. In Fig. 11, after $s_s\left(t\right)$ is shifted by Δf and Δt, a segment of the TF spectrogram (from point *a* to point *b*) of $s_s\left(t\right)$ becomes coincident with part (from point *c* to point *d*) of $s_r\left(t\right)$, and for this case, there appears a maximum cross-correlation peak between $s_s(t)$ and $s_r(t)$.

In addition, $f_s(t+\Delta t)$ does not change the shape of the TF spectrogram of $f_s(t)$, and only causes a shift of the spectrogram along the time axis. In other words, the Doppler mismatch of $s_r(t)$ is only caused by Δf according to (20). Therefore, to solve the mismatch issue between $s_s(t)$ and $s_r(t)$, and then obtain a maximum cross-correlation peak between $s_s(t)$ and $s_r(t)$, we only need to accurately compensate Δf through the shift of carrier frequency f_c.

B. Speed and range estimation

In the proposed method, we use a single signal waveform to measure the range of the target and a combination of two signal waveforms with low cross-correlation between them to estimate the speed of the target, as shown in Fig. 12.

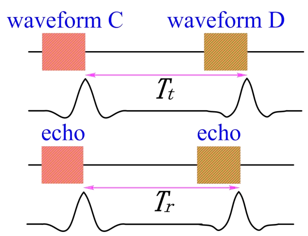

Fig. 12. Doppler speed measurement principle when the sonar system and the target move in opposite directions.

Based on the Doppler speed measurement principle, the following relationship can be obtained:

$$T_r = \frac{c-v}{c+v} T_t = \alpha T_t \approx (1-2v/c) T_t \tag{21}$$

where T_t is the time difference between the transmitted waveform C $s_{s,C1}(t)$ and waveform D $s_{s,D1}(t)$, T_r is the time difference between the return echo $s_{e,C}(t)$ of waveform C and the return echo $s_{e,D}(t)$ of waveform D.

Further, based on (21), the speed of the target can be estimated through

$$v \approx (T_t - T_r) \cdot c / 2T \tag{22}$$

In order to obtain an accurate estimate v' of the speed v, a good estimate T_r' for T_r needs to be obtained. In the following, a three-step estimation process of T_r' is presented.

First Step: Assume that at time t_1, the end of the return echo of waveform C arrives at the sonar receiver; at time t_2, the end of the return echo of waveform D arrives at the sonar receiver; the time difference between the end of waveform C and the end of waveform D is T_t; the time difference between the end of the return echo of waveform C and the end of the return echo of waveform D is T_r. Then,

$$T_r = t_2 - t_1 \tag{23}$$

t_1 can be estimated through the cross-correlation peak between waveform C and its return echo signal, and the estimation is denoted by $\overline{t}_{C1}(\Delta f_C)$, which is a function of Δf_C. Likewise, t_2 can be estimated through the cross-correlation peak between waveform D and its return echo signal, and the estimation is denoted by $\overline{t}_{D1}(\Delta f_D)$.

The accuracy of $\overline{t}_{C1}(\Delta f_C)$ depends on the degree of mismatch between waveform C and its return echo signal; when the degree of mismatch is large, the accuracy of $\overline{t}_{C1}(\Delta f_C)$ will be low; on the contrary, the better the mismatch is compensated, the more accuracy of $\overline{t}_{C1}(\Delta f_C)$ will become. The same is true for $\overline{t}_{D1}(\Delta f_D)$.

Meanwhile, the following relationships can be obtained

$$\begin{aligned} T_{r1} &= \overline{t}_{D1}(\Delta f_D) + \Delta t_D - [\overline{t}_{C1}(\Delta f_C) + \Delta t_C] \\ &= \overline{t}_{D1}(\Delta f_D) - \overline{t}_{C1}(\Delta f_C) + (\Delta t_D - \Delta t_C) \end{aligned} \tag{24}$$

where T_{r1} is a coarse estimation of T_r without compensation of the Doppler effect; Δt_C and Δt_D are the time shifts corresponding to waveforms C and D, respectively; Δf_C and Δf_D are the corresponding frequency shifts. And Δt_C and Δt_D are obtained by (25) and (26) based on (11), $\alpha \approx 1-2v/c$ and $b = (f_L - f_H)/(f_L f_H T)$.

$$\Delta t_C = (1-\alpha)/\alpha b_C f_{L_C} = f_{H_C} T_C (\alpha - 1)/(f_{L_C} - f_{H_C})\alpha \tag{25}$$

$$\Delta t_D = (1-\alpha)/\alpha b_D f_{L_2} = f_{H_D} T_D (\alpha - 1)/(f_{L_D} - f_{H_D})\alpha \tag{26}$$

where $b_C = (f_{L_C} - f_{H_C})/(f_{L_C} f_{H_C} T_C)$, $b_D = (f_{L_D} - f_{H_D})/(f_{L_D} f_{H_D} T_D)$, f_{L_C} and f_{H_C} are the start frequency and the end frequency of waveform C, respectively, f_{L_D} and f_{H_D} are those of waveform D, T_C is the duration of waveform C and T_D is the duration of waveform D.

Δf_C and Δf_D are obtained by (27) and (28) based on (10).

$$\Delta f_C = (\alpha - 1) f_{c,C} \tag{27}$$

$$\Delta f_D = (\alpha - 1) f_{c,D} \tag{28}$$

where $f_{c,C}$ and $f_{c,D}$ are the part of carrier frequencies corresponding to waveforms C and D, respectively.

Since Δf_C and Δf_D are functions about α, and Δt_C and Δt_D are also functions about α, (24) can be rewritten as

$$T_{r1} = \overline{t}_{D1}[\Delta f_D(\alpha_1)] - \overline{t}_{C1}[\Delta f_C(\alpha_1)] + [\Delta t_D(\alpha_1) - \Delta t_C(\alpha_1)] \tag{29}$$

where α_1 denotes the true Doppler scale factor caused by the relative speed v.

Since α_1 is unknown, the values of $\Delta t_C(\alpha_1)$ and $\Delta t_D(\alpha_1)$ cannot be obtained yet. Considering that both waveforms C and

D have excellent Doppler tolerance, rough estimations T_{r2} of T_{r1} can be obtained by ignoring $\Delta t_C(\alpha_1)$ and $\Delta t_D(\alpha_1)$.

$$T_{r2} = \overline{t}_{D1}[\Delta f_D(\alpha_1)] - \overline{t}_{C1}[\Delta f_C(\alpha_1)] \tag{30}$$

$\overline{t}_{C1}[\Delta f_C(\alpha_1)]$ can be estimated by computing the cross-correlation between waveform C and its return, and $\overline{t}_{D1}[\Delta f_D(\alpha_1)]$ can be estimated in the same way. Most importantly, the estimated $\overline{t}_{C1}[\Delta f_C(\alpha_1)]$ is coarse due to a large mismatch between waveform C and its return. The same is true for $\overline{t}_{D1}[\Delta f_D(\alpha_1)]$.

Substituting (30) into (21), a coarse estimate α_2 for α_1 can be obtained.

$$\alpha_2 = T_{r2} / T_t \tag{31}$$

Second Step: Substituting α_2 into (25), (26), (27) and (28), we can obtain coarse estimations $\Delta t_C(\alpha_2)$, $\Delta t_D(\alpha_2)$, $\Delta f_C(\alpha_2)$ and $\Delta f_D(\alpha_2)$ for $\Delta t_C(\alpha_1)$, $\Delta t_D(\alpha_1)$, $\Delta f_C(\alpha_1)$ and $\Delta f_D(\alpha_1)$, respectively.

Given (20) and relevant results in Section V-A, after waveform C $s_{s,C1}(t)$ is shifted by $\Delta f_C(\alpha_2)$, $s_{s,C1}(t)$ becomes $s_{s,C2}(t)$

$$s_{s,C1}(t) = A_C(t)\exp[j2\pi(\frac{1}{b_C}\ln(1+b_C f_{L_C} t) + f_{c,C}t + \Delta f_{C,1}(\alpha_2)t)] \tag{32}$$

and the matching between $s_{s,C2}(t)$ and $s_{e,C}(t)$ will be better than that between $s_{s,C1}(t)$ and $s_{e,C}(t)$, because part of the carrier frequency is compensated preliminarily. In other words, the cross-correlation peak between $s_{s,C2}(t)$ and $s_{e,C}(t)$ will be larger and more accurate than the cross-correlation peak between $s_{s,C1}(t)$ and $s_{e,C}(t)$. Likewise, the cross-correlation peak between $s_{s,D2}(t)$ and $s_{e,D}(t)$ will be larger than that between $s_{s,D1}(t)$ and $s_{e,D}(t)$.

Further, assume that the estimated time corresponding to the cross-correlation peak between the waveform $s_{s,C2}(t)$ and the return echo $s_{e,C}(t)$ of waveform C is $\overline{t}_{C1}[\Delta f_C(\alpha_2)]$, and the estimated time corresponding to the cross-correlation peak between the waveform $s_{s,D2}(t)$ and the return echo $s_{e,D}(t)$ of waveform D is $\overline{t}_{D1}[\Delta f_C(\alpha_2)]$. According to (29), one can obtain

$$T_{r3} = \overline{t}_{D1}[\Delta f_D(\alpha_2)] - \overline{t}_{C1}[\Delta f_C(\alpha_2)] + [\Delta t_D(\alpha_2) - \Delta t_C(\alpha_2)] \tag{33}$$

Because $\overline{t}_{C1}[\Delta f_C(\alpha_2)]$ and $\overline{t}_{D1}[\Delta f_C(\alpha_2)]$ are more accurate than $\overline{t}_{C1}[\Delta f_C(\alpha_1)]$ and $\overline{t}_{D1}[\Delta f_C(\alpha_1)]$, respectively, and the coarse estimations $\Delta t_C(\alpha_2)$ and $\Delta t_D(\alpha_2)$ of $\Delta t_C(\alpha_1)$ and $\Delta t_D(\alpha_1)$ can be computed by the estimated α_2 (see (31)), one can obtain a more accurate estimation T_{r3} of T_r than T_{r2} based on (33).

Then, similar to (31), a more accurate estimation value α_3 than α_2 can be obtained

$$\alpha_3 = T_{r3} / T_t \tag{34}$$

Third Step: Similar to the processing procedure above the **Second Step**, a more accurate estimation T_{r4} than T_{r3} can be obtained

$$T_{r4} = \overline{t}_{D1}[\Delta f_D(\alpha_3)] - \overline{t}_{C1}[\Delta f_C(\alpha_3)] + [\Delta t_D(\alpha_3) - \Delta t_C(\alpha_3)] \tag{35}$$

And a more accurate estimation α_4 than α_3 is given by

$$\alpha_4 = T_{r4} / T_t \tag{36}$$

Repeating the above process multiple times, one can obtain

$$T_{rN} = \overline{t}_{D1}[\Delta f_D(\alpha_{(N-1)})] - \overline{t}_{C1}[\Delta f_C(\alpha_{(N-1)})] + [\Delta t_D(\alpha_{(N-1)}) - \Delta t_C(\alpha_{(N-1)})] \tag{37}$$

$$\alpha_N = T_{rN} / T_t \tag{38}$$

The larger N is, the closer $T_{rN} = T_r'$ and α_N are to T_r and α_1, respectively, and N can be decided according to the estimation error requirement. This is an iterative process and the estimation accuracy improves as the number of iterations increases.

Finally, based on (22), the speed of the target can be estimated

$$v' \approx (T_t - T_{rN})c / 2T_t \tag{39}$$

The estimation value R' for range R can be obtained by

$$R' \approx \{\overline{t}_{C1}[\Delta f_C(\alpha_{(N-1)})] - t_0\}c / 2 \tag{40}$$

where t_0 denotes the time instant that the end of waveform C is sent out from the sonar system.

VI. Possible Camouflage Application Strategy

In a real world, false killer whales can produce various clicks and whistles from time to time [28-30]. If the sonar system only transmits the same combination composed of two bionic sonar signal waveforms from time to time, the lack of diversity will generate an obvious repetitive feature distinctive from that of a true false killer whale. This is because that the bionic sonar signal waveforms are only constructed according the whistles of false killer whales instead of clicks.

In order to solve the above issues and improve the camouflage ability of target detection process, a possible camouflage application strategy is designed as shown in Fig. 13.

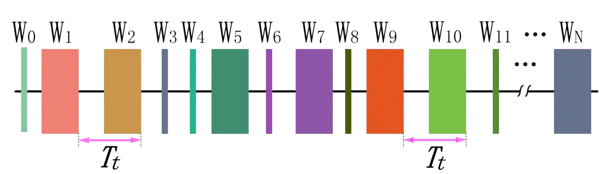

Fig. 13. Possible camouflage application strategy.

In Fig. 13, W_1, W_2, W_9 and W_{10} are the bionic sonar signal waveforms. W_1 and W_2 form a combination, W_9 and W_{10} form another one, and these combinations are used to estimate the range and speed of targets based on the measurement principle in Section V-B. W_0, W_3, W_4, W_6, W_8 and W_{11} are the true false killer whale clicks, and W_5, W_7 and W_N are the true false killer whale whistles selected randomly from Type-2, Type-3, Type-4, Type-5 or Type-6. These clicks and whistles are used to disguise the constructed bionic sonar signal waveforms, and called “camouflage cloak”. No click is present between two constructed bionic sonar signal waveforms which form a combination, such as between W_1 and W_2. But one or more clicks can be added between one bionic sonar signal waveform and another true whistle (such as W_2 and W_5), or between two true whistles (such as W_5 and W_7).

According to the above camouflage application strategy, one can know that all constructed bionic sonar signal waveforms, all true whistles and all clicks are different from each other. That is to say, there is no obvious repetitive feature in the signal pulse sequence in Fig. 13, which can improve the camouflage ability of the sonar signal sequence. In addition, other types of whistles (namely Tpye-2, Tpye-3, Tpye-4, Tpye-5 and Tpye-6) and different true clicks are used in the sonar signal sequence in Fig.13, which can increase the diversity of whistles and clicks, and further improve the camouflage ability of the sonar signal sequence. It can be see from Fig.14 that the sonar signal sequence is very close to the true call train of false killer whales.

Since there are no clicks between the two constructed bionic sonar signal waveforms, while there are one or multiple clicks between the bionic sonar signal waveform and another true whistle, or between two true whistles, the two constructed bionic sonar signal waveforms can be identified and decoded when there are no clicks between two long-duration call pulses (namely bionic whistle or true whistle). For visualization, a segment of a constructed bionic sonar signal sequence is shown in Fig. 14.

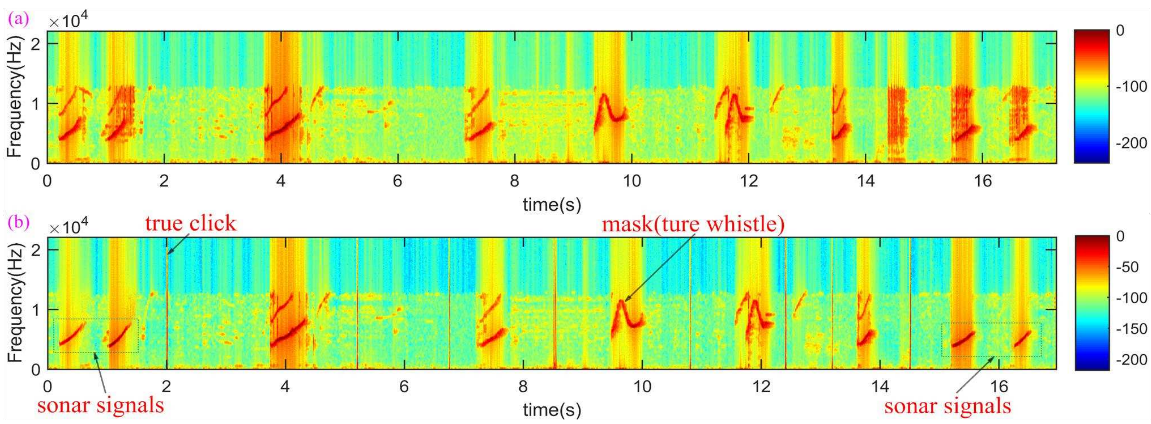

Fig. 14. (a) The TF spectrogram of the true call train, (b) the TF spectrogram of the constructed bionic sonar signal sequence.

On the one hand, the constructed bionic sonar signal waveforms are very close to the true false killer whale whistles in terms of time domain waveform, frequency distribution and TF distribution; on the other hand, complying with the characteristic of the inter-pulse interval of the false killer whale true call train, the constructed bionic sonar signal waveforms and the “camouflage cloak” are formed into a new sonar signal sequence, which ensures that the inter-pulse interval of the constructed sonar signal sequence is consistent with the false killer whale true call train.

The conventional methods achieve the covert operation for active sonar detection by reducing the SNR of the transmitted sonar signals. This is because that it is very difficult for the enemy’s interception systems to detect the low SNR signals. However, the proposed method achieves the covert operation through camouflage strategy. That is to say, based on the fact that the present interception systems almost always classify biological signals as ocean noise and try to filter them out [25-27], the proposed method uses the constructed bionic sonar signal waveforms (they are very like the true whale call) to serve as the sonar signals, and thus achieves the covert operation through camouflage strategy. Further, by employing the proposed bionic sonar signal waveforms, although high SNR sonar signals have to be used for long range detection, the covertness of the system will not be affected significantly. On the other hand, when facing a short range target detection task, the system can achieve further improved covertness by reducing the SNR of the transmitted bionic sonar signals similar to the principle of conventional methods which use low SNR signals for covert operation.

It is noteworthy that although no click is placed between two constructed bionic sonar signal waveforms, this does not affect the camouflage performance of the constructed bionic sonar signal waveform; this is because that in the true false killer whale call trains, there exit similar whistle waveforms between which there is no click; meanwhile, there are also many whistle waveforms between which there is one or multiple clicks.

VII. REMARKS

What is noteworthy is that the proposed camouflage technology should be used in some sea area where the false killer whales exist or people do not sure if the false killer whales exist. In fact, the fake killer whales live widely in the world's major oceans except the Arctic Ocean, and thus the scope and sea area of application of the proposed camouflage strategy is extensive.

In addition, the proposed disguised bionic sonar signal waveform design method may not be perfect, but it is an interesting attempt and can enlighten other researchers to further research and improve this kind of disguised bionic sonar signal waveform design method, and explore the relevant technology by using other whale species.

VIII. Simulations and Experiments

A. Speed and range estimation

In this section, we examine the performance of the proposed method through computer simulations.

Please note that the existing conventional methods are to design covert sonar signal waveforms by changing the parameters or suppressing the SNR of sonar signal waveforms, however, in this paper, the proposed method is an entirely different and new method, and is to design covert sonar signal waveforms by using the true whale calls (disguised bionic sonar signal waveform). In other words, under the same conditions, it is very difficult or even impossible to compare the covert performance of designed sonar signal waveforms between the existing conventional methods based on parameter-changing or low SNR signals and the proposed method based on the disguised bionic sonar signal waveform. Therefore, in the following simulations and experiments, we only evaluate the performance of the proposed method from multiple aspects instead of comparison with other existing conventional methods.

The underwater acoustic channel (WATTCH) model in [39] is used to simulate the practical oceanic environment. The modeling starts with calculating the fast Fourier transform (FFT) of the sonar waveform, which yields the frequency-dependent amplitude and phase representation of the waveform. A set of eigen-rays is then generated through BELLHOP [40-41], and they represent all of the significant contributing acoustic paths between the source and the receiver [42]. Seawater density, seafloor density and wind speed are set to be 1.024 g/cm^3, 1.469 g/cm^3 and 5m/s, respectively. The target moves at a relative speed of $v = 5\text{m/s}$ away from the sonar system source. Other key parameters are shown in Fig. 15, with the sound speed profile for the simulated shallow-water model given in Fig. 16.

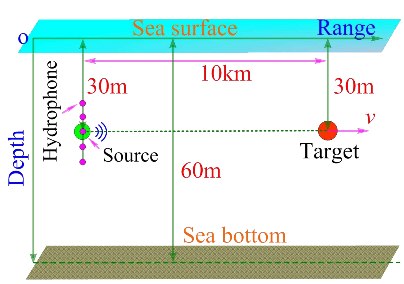

Fig. 15. Simulation setup

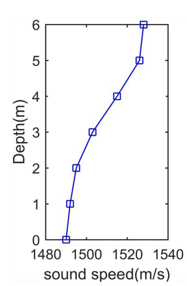

Fig. 16. Sound speed profile

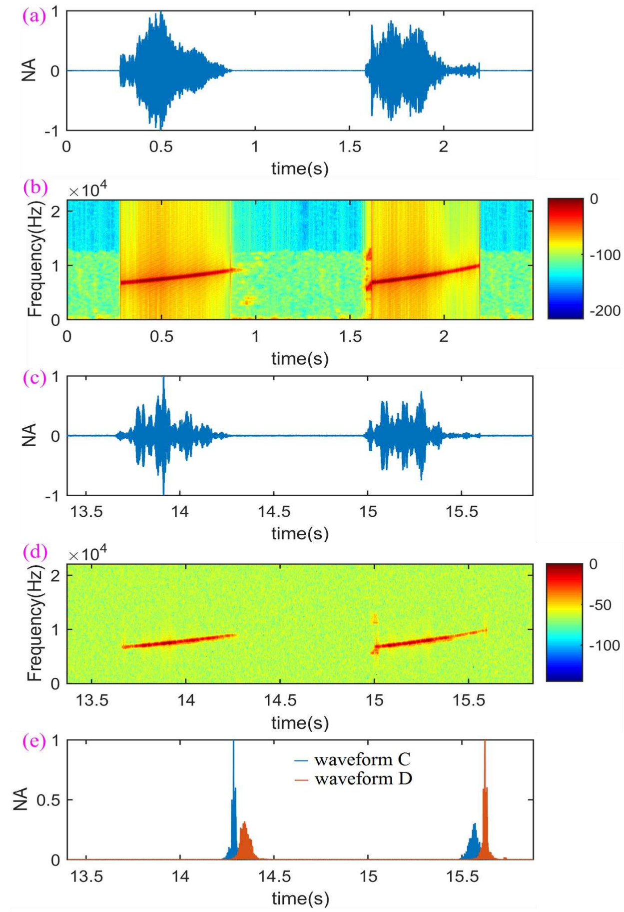

Fig. 17. (a) A combination waveform composed of two constructed bionic sonar signal waveforms C and D, (b) the TF spectrogram of the constructed combination, (c) the two received return echoes, (d) their TF spectrogram, (e) the estimated time difference between the two received return echoes after three iterations.

In the first simulation, the constructed bionic sonar signal waveforms C and D (Fig. 17(a)) are used to form a combination to measure the range and speed of the target. Their TF spectrograms are shown in Fig. 17(b). The combination is transmitted at an SNR of 10dB. Assume that the reflection coefficient of the target is one. After the waveforms pass through the underwater acoustic channel, they are reflected by the target, through the underwater acoustic channel again, and then their return echoes arrive at the sonar receiving system. Fig. 17(c) shows the received return echoes, which have a different time domain envelope from the transmitted waveforms C and D owing to the impact of the underwater acoustic channel. Fig. 17(d) shows the TF spectrogram of the received return echoes. Using the range and speed estimation methods presented in Section V, the time length of sonar waveforms arriving at the target and then coming back to the sonar receiving system and the time difference between the received two return echoes are obtained, respectively, and then the estimated range and speed of the target are obtained.

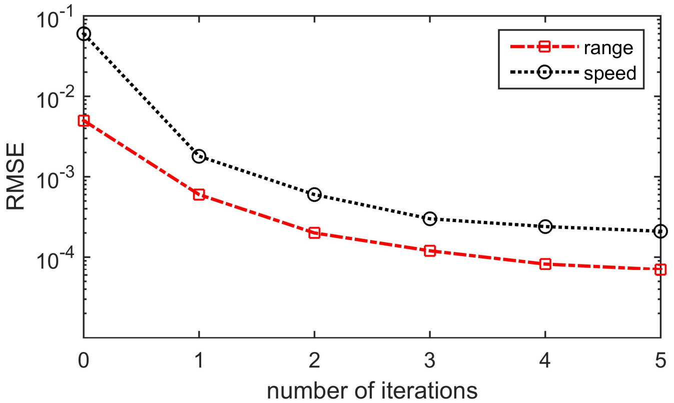

Fig.18. The RMSE of the estimated range and speed with SNR=10dB for the transmitted sonar signal waveforms.

Next, fixing the SNR of the transmitted sonar signal waveforms at 10dB, the effect of the number of iterations (please see (37)-(40)) on the estimation accuracy for range and speed is examined. The root-mean-square error (RMSE) results [43] of the estimated range and speed with 100 independent Monte Carlo runs [43-44] are shown in Fig. 18. It can be seen that with the increase of the number of iterations, the estimation accuracy improves continuously. However, the first three iterations have the most impact on the result, while the improvement becomes less beyond that. This indicates that in practice, for a low-complexity implementation, three iterations could be employed with a satisfactory performance.

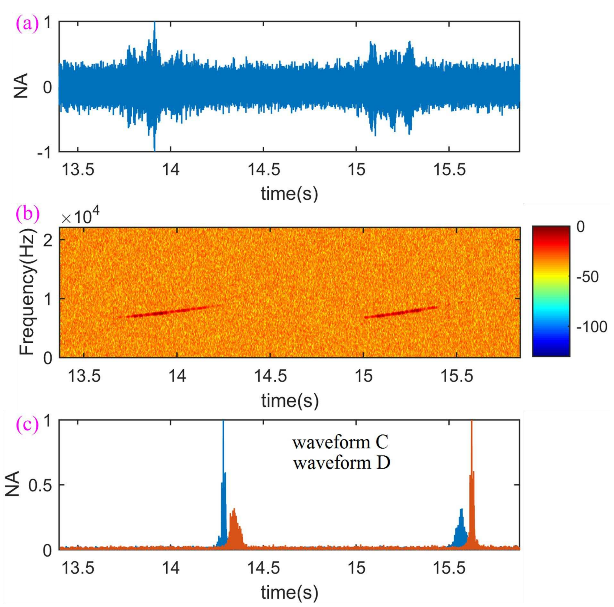

Fig. 19. (a) Waveforms of the two received return echoes, (b) their TF spectrogram, (c) the estimated time difference between the two received return echoes after three iterations.

In the second simulation, the low SNR case is evaluated and the SNR of the transmitted sonar signal waveforms is set to -10dB. All other parameters are the same as in the first simulation. The combination of two constructed bionic sonar signal waveforms C and D is transmitted. Fig. 19 shows the waveforms of the two received return echoes, their TF spectrogram and the estimated time difference between the two received return echoes after three iterations. It can be seen that even at a low SNR value, a high estimation performance can still be achieved by the proposed method.

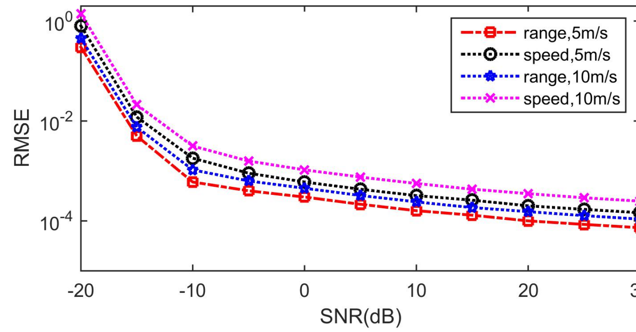

Fig. 20. Estimation performance of the range and speed at different SNRs and different speeds of the target.

In the third simulation, the estimation performance is evaluated as the SNR varies from -20dB to 30dB on the condition that the speed of the target is 5m/s and 10m/s, respectively. Other simulation parameters are the same as in the first simulation. The RMSE results with 100 independent Monte Carlo runs are shown in Fig. 20, where it can be seen that as the SNR increases, the RMSE of the estimated range and speed decreases continuously. The estimation performance under the target's speed of 5m/s is superior to that of 10m/s, which is because that the return echoes under a speed of 10m/s have larger deformation caused by the Doppler effect, and thus results in that the cross-correlation results have larger errors.

B. Camouflage ability evaluation

In the fourth experiment, the camouflage ability of the constructed waveforms is examined. Support Vector Machine (SVM), which is widely used in small sample recognition problems and underwater acoustic signal recognition [45], was used as classifier to classify the constructed bionic sonar signal waveforms and the first type of true whistles in Table 1. We utilized the five order polynomials to fit the ridge of the TFs of both the constructed sonar signal waveforms and the first type of true whistles, and then five coefficients and residual error of the five order polynomials were used as feature parameters to train the classifier. K-fold cross-validation is a traditional and effective method to evaluate the performance of a classifier over a dataset [46-47]. In this paper, 4-fold cross-validation was used for classification evaluation, 80 false killer whale whistles were randomly partitioned into four equal sized datasets W_{S1}, W_{S2}, W_{S3} and W_{S4}, and each of the four datasets contains 20 whale whistles. Likewise, 80 constructed bionic sonar signal waveforms were also randomly divided into four equal sized datasets S_{S1}, S_{S2}, S_{S3} and S_{S4}. In each cross-validation process, a subsample, which included three sets of the whale whistles and three sets of the sonar signal waveforms, was used as training data for the SVM classifier, and then the remaining whale whistles and sonar signal waveforms were classified and recognized by the SVM classifier. The cross-validation process is then repeated three times, and each group of the whale whistles (namely W_{S1}, W_{S2}, W_{S3} and W_{S4}) and sonar signal waveforms (namely S_{S1}, S_{S2}, S_{S3} and S_{S4}) were used once as the classified data.

Table 2.Confusion matrices' results of the four-fold cross-validation of SVM classifiers

Classifier serial number	Training data	Classified data		Sonar signals (%)	Whale whistles (%)
1	W_{S1}, W_{S2}, W_{S3}, S_{S1}, S_{S2}, S_{S3}	W_{S4}, S_{S4}	Sonar signals	50	50
			Whale whistles	55	45
2	W_{S1}, W_{S2}, W_{S4}, S_{S1}, S_{S2}, S_{S4}	W_{S3}, S_{S3}	Sonar signals	35	65
			Whale whistles	25	75
3	W_{S1}, W_{S3}, W_{S4}, S_{S1}, S_{S3}, S_{S4}	W_{S2}, S_{S2}	Sonar signals	35	65
			Whale whistles	45	55
4	W_{S2}, W_{S3}, W_{S4}, S_{S2}, S_{S3}, S_{S4}	W_{S1}, S_{S1}	Sonar signals	50	50
			Whale whistles	45	55

Table 2 shows the experimental conditions and confusion matrices' results of the four-fold cross-validation of SVM classifiers. For the first SVM classifier, 50% of S_{S4} were classified as the bionic sonar signal waveforms and 45% of W_{S4} were classified as the whale whistles. Therefore, the classification rate of the first SVM classifier is (50%*20+45%*20)/(20+20)=47.5%. Similarly, the classification rates of the remaining three SVM classifiers are 55.0%, 45.0% and 52.5%, respectively. Based on above results, one can see that the bionic sonar signal waveforms have an about 50% probability of being classified as the true whale whistles, and the true whistles of false killer whales also have an about 50% probability of being classified as the bionic sonar signal waveforms, which indicates that the SVM classifier cannot distinguish the bionic sonar signal waveforms from the true whistles of false killer whales, that is to say, the constructed bionic sonar signal waveforms are very close to the true whistle of false killer whales.

IX. CONCLUSION

Different from conventional parameter-changing or low SNR sonar signal waveforms for covert operations, a new type of bionic sonar signal waveform design with its possible camouflage application strategy has been proposed by highly imitating the false killer whale whistles to construct the bionic and disguised sonar signal waveforms. According to the time resolution and Doppler tolerance of the proposed bionic sonar signal waveforms, a computationally efficient target range and speed estimation algorithm was developed and evaluated. The covertness of the constructed sonar signal waveforms and their camouflage application strategy were designed and improved from multiple aspects (time domain waveform, frequency distribution, TF distribution, inter-pulse interval and diversity of the signal waveforms). Most important of all, the proposed approach can solve the trade-off problem between long-range detection and covertness. It can keep a satisfactory level of covertness by means of camouflage even if the SNR of the transmitted signals is very high. On the other hand, it can improve the covertness further by reducing the SNR for a short range target detection task. The proposed bionic sonar signal waveform design technology can be used widely in the underwater sensor platforms.

In this paper, only 80 Type-1 whistles are imitated. In the future research work, other types of whistles will be imitated through in-depth studies.

X. ACKNOWLEDGMENTS

This work was supported in part by the TianJin Natural Science Foundations of China under Grant No. 17JCQNJC01100, National Natural Science Foundations of China under Grant No. 61501319, 51775377, 61505140, National key research and development plan (2017YFF0204800), Young Elite Scientists Sponsorship Program By Cast of China under Grant No. 2016QNRC001, Open Project (MOMST2015-7) of Key Laboratory of Micro Opto-electro Mechanical System Technology, Tianjin University, Ministry of Education, Photoelectric Information and Instrument-Engineering Research Center of Beijing Open Project No.GD2015007.

REFERENCE

[1] Follett, R. F., and J. P. Donohoe. "A wideband, high-resolution, low-probability-of-detection FFT beamformer." *IEEE Journal of Oceanic Engineering*, vol.19, no.2, pp.175-182, 1994.

[2] Nicholson, David L. "Spread spectrum signal design: LPE and AJ systems." (1988).

[3] Lourey, Simon J. "Frequency hopping waveforms for continuous active sonar." *IEEE International Conference on Acoustics, Speech and Signal Processing*, pp.1832-1835, 2015.

[4] Keerthi, Y. and TD Bhatt. "LPI radar signal generation and detection", 2015.

[5] Stanciu, Mihai Ionut, S. Azou, and A. Serbanescu. "On the blind estimation of chip time of time-hopping signals through minimization of a multimodal cost function." *IEEE Transactions on Signal Processing,* vol.59, no.2, pp, 842-847, 2011.

[6] Marszal J, Salamon R. "Detection range of intercept sonar for CWFM signals." *Archives of Acoustics*, vol.39, no.2, pp.215-230, 2014.

[7] Marszal J, Salamon R, Kilian L. "Application of maximum length sequence in silent sonar." *Hydroacoustics*, vlo.15, pp.143-152, 2012.

[8] Marszal J, Salamon R, Zachariasz K, et al. "Doppler effect in the cw fm sonar." *Hydroacoustics*, vol.14, pp. 157-164, 2011.

[9] Kulpa K, Lukin K, Miceli W, et al. "Signal processing in noise radar technology [Editorial]." *IET Radar, Sonar & Navigation*, vol.2, no.4, pp.229-232, 2008.

[10] Lynch R S, Willett P K, Reinert J M. "Some analysis of the LPI concept for active sonar." *IEEE Journal of Oceanic Engineering*, vol.37, no.3, pp. 446-455, 2012.

[11] Iglesias, V, et al. "Real-time low-complexity automatic modulation classifier for pulsed radar signals." *IEEE Transactions on Aerospace & Electronic Systems,* vol.51, no.1, pp.108-126, 2015.

[12] Shui, Peng Lang, Z. Bao and H. T. Su. "Nonparametric detection of FM signals using time-frequency ridge energy." *IEEE Transactions on Signal Processing,* vol. 56, no.5, pp.1749-1760, 2008.

[13] Learned R. E., Willsky A. S. "A wavelet packet approach to transient signal classification." *Applied and Computational Harmonic Analysis*, vol.2, no.3, pp.265-278, 1995.

[14] Morrissey R P, Ward J, DiMarzio N, *et al.* "Passive acoustic detection and localization of sperm whales (Physeter macrocephalus) in the tongue of the ocean," *Applied acoustics*, vol.67, no.11, pp.1091-1105, 2006.

[15] Wu, Linlong, P. Babu, and D. P. Palomar. "Transmit waveform/receive filter design for MIMO radar with multiple waveform constraints." *IEEE Transactions on Signal Processing*, vol.66, no.6, pp. 1526-1540, 2017.

[16] Tang, Bo, M. M. Naghsh, and J. Tang. "Relative entropy-based waveform design for MIMO radar detection in the presence of clutter and interference." *IEEE Transactions on Signal Processing*, vol.63, no.14, pp.3783-3796, 2015.

[17] Cheng, Ziyang, *et al.* "Constant modulus waveform design for MIMO radar transmit beampattern." *IEEE Transactions on Signal Processing*, vol.65, no.18, pp.4912-4923, 2017.

[18] Mueller, R., Kuc, R.: 'Biosonar-inspired technology: goals, challenges and insights', *Bioinspiration & Biomimetics*, vol.2, no.4, pp), pp. 146-61, 2007.

[19] Capus, C, *et al.* "Bio-inspired wideband sonar signals based on observations of the bottlenose dolphin (Tursiops truncatus)." *Journal of the Acoustical Society of America,* vol. 121, no.1, pp.594-604, 2007.

[20] Leighton, Timothy, and P. White. "Dolphin-Inspired Target Detection for Sonar and Radar." *Archives of Acoustics*, vol.39, no.3, pp. 319-332, 2015.

[21] Jiajia Jiang, Xianquan Wang, *et al.*, "Bio-inspired steganography for secure underwater acoustic communications." *IEEE Communication Magazine*, Have been accepted for publish.

[22] Dobbins P. "Dolphin sonar--modelling a new receiver concept." *Bioinspiration & Biomimetics*, vol.2, no.1, pp.19-29, 2007.

[23] Bryan D Todd and Rolf Müller, "A comparison of the role of beamwidth in biological and engineered sonar" *Bioinspiration & Biomimetics, vol.*13, pp.016014, 2018.

[24] Vespe, M, G. Jones, and C. J. Bakers. "Lessons for radar waveform diversity in echolocating mammals." *IEEE Signal Processing Magazine*, vol. 26, no.1, pp.65-75, 2009.

[25] Ijsselmuide, S. P. Van, and S. P. Beerens. "Detection and classification of marine mammals using an LFAS system." *Journal of Thoracic Oncology,* vol. 32, no.2, pp.417-424, 2004.

[26] Chen, Chin Hsing, L. Jiann-Der, and M. C. Lin. "Classification of underwater signals using wavelet transforms and neural networks." *Mathematical & Computer Modelling,* vol. 27, no.2, pp.47-60, 1998.

[27] Papandreou-Suppappola, A, and S. B. Suppappola. "Analysis and classification of time-varying signals with multiple time-frequency structures." *IEEE Signal Processing Letters, vol.*9, no.3, pp.92-95, 2015.

[28] Brill, R. L., *et al.* "Target detection, shape discrimination, and signal characteristics of an echolocating false killer whale (Pseudorca crassidens)." *Journal of the Acoustical Society of America*, vol. 92, no.3, pp.1324-1330, 1992.

[29] Au, Whitlow W. L., *et al.* "Echolocation signals and transmission beam pattern of a false killer whale (Pseudorca crassidens)." *Journal of the Acoustical Society of America*, vol. 98, no.1, pp.51-59, 1995.

[30] Rendell, L. E., et al. "Quantitative analysis of tonal calls from five odontocete species, examining interspecific and intraspecific variation." *Proceedings of the Zoological Society of London*, vol. 249, no.4, pp.403-410, 1999.

[31] Calderon, M. A. "Probability density analysis of ocean ambient and ship noise." *Navy Electronics Lab San Diego Calif*, 1964.

[32] Ephraim, Y., and D. Malah. "Speech enhancement using a minimum mean-square error log-spectral amplitude estimator." *IEEE Transactions on Acoustics Speech & Signal Processing*, vol. 32, no.2, pp.443-445, 1984.

[33] Wilpon, J. G., L. R. Rabiner, and T. Martin. "An improved word-detection algorithm for telephone-quality speech incorporating both syntactic and semantic constraints." *At & T Bell Laboratories Technical Journal*, vol.63, no.3, pp.479-498, 2014.

[34] Yang, J. and T.K.Sarkar. "Doppler-invariant property of hyperbolic frequency modulated waveforms" *Microwave and Optical Technology Letter*, vol.48, no.6, pp.1174-1179, 2006.

[35] Harris, F. J. "On the use of harmonic analysis with the discrete Fourier transform." *Proc IEEE*, vol. 66, no.1, pp.51-83, 1978.

[36] Wehner, Donald R. "High resolution radar." *Norwood Ma Artech House Inc*, 1995.

[37] Weiss L G. "Wavelets and wideband correlation processing." *IEEE Signal Processing Magazine*, vol.11, no.1, pp.13-32, 1994.

[38] Kelly, E. J, and R. P. Wishner. "Matched-filter theory for high-velocity, accelerating targets." *IEEE Transactions on Military Electronics, vol.* 9, no.1, pp.56-69, 1965.

[39] Pecknold, S, et al. "Time-series modeling using the waveform transmission through a channel program." *Oceans 2005- Europe, vol.*2, pp.993-1000, 2005.

[40] M. B. Porter, "The bellhop manual and users guide: preliminary draft," *Heat, Light, and Sound Research, Inc.*, La Jolla, CA, USA, Tech. Rep, 2011.

[41] Mccammon, Diana. "Active acoustics using Bellhop-DRDC: run time tests and suggested configurations for a tracking exercise in shallow scotian waters." *Archives of Biochemistry & Biophysics*, vol.68, no.2, pp.507-509, 2005.

[42] Jensen, F. "Numerical models of sound propagation in real oceans." *Oceans* IEEE, vol.147-154, 1982.

[43] Jiang Jia-jia, Duan Fajie, Chen Jin, Li Yanchao, Hua Xiangning. Mixed near-field and far-field sources localization using the uniform linear sensor array. *IEEE Sensors Journal*, vol 13, no. 8, pp.3136-3143, 2013.

[44] Jiang Jia-jia, Duan Fajie, Chen Jin, Zhang Chao, Chang Zongjie, Hua Xiangning. Two new estimation algorithms for sensor gain and phase errors based on different data models. *IEEE Sensors Journal*, vol.13, no. 5, pp.1921-1930, 2013.

[45] Zhang, Xinhua, Z. Lu, and C. Kang. "Underwater acoustic targets classification using support vector machine." *IEEE International Conference on Neural Networks and Signal Processing*, vol.2, pp.932-935, 2004.

[46] Kohavi, Ron. "A study of cross-validation and bootstrap for accuracy estimation and model selection." *International Joint* Conference on Artificial Intelligence, pp.1137-1143, 1995

[47] Sunny, Kumar V, Mishra V N, et al. Classification and quantification of binary mixtures of gases/odors using thick-film gas sensor array responses. *IEEE Sensors Journal*, 2014, 15(2):1252-1260.

Jiajia Jiang was born in HuBei, China, in 1986. He received the B.S. degrees from HeBei Normal University and the M.S. degree and Ph.D. degree from TianJin University (State Key Lab of Precision Measuring Technology & Instruments), TianJin, China, in 2011 and 2014, respectively. He is currently an associate professor in TianJin University (State Key Lab of Precision Measuring Technology & Instruments).
His research interest focuses on underwater acoustic detection, underwater acoustic communication, array signal processing.

Zhongbo Sun was born in HuBei, China, in 1993. He received the B.S. degree from Liaoning University, Shenyang, China in 2016. He is currently working toward a M.S. degree in State Key Lab of Precision Measuring Technology and Instruments at TianJin University.
His research interest focuses on the underwater acoustic detection and communication.

Fajie Duan was born in HuNan, China, in 1968. He received the M.S. degrees from TianJin University and the Ph.D. degree from TianJin University (State Key Lab of Precision Measuring Technology & Instruments), TianJin, China, in 1991 and 1994, respectively.He worked as a professor at TianJin University (State Key Lab of Precision Measuring Technology & Instruments) since 2004.
His research interest focuses on the design of the array system, array signal processing, acoustic detection of marine. He was named the National New Century Excellent Talents of Ministry of Education in 2005. He is the author or coauthor of over 120 papers and holds seven patents.

Wei Liu received the B.Sc. and L.L.B. degrees from Peking University, China, in 1996 and 1997, respectively, the M.Phil. degree from The University of Hong Kong in 2001, and the Ph.D. degree from the School of Electronics and Computer Science, University of Southampton, U.K., in 2003. He held a post-doctoral position at the Imperial College London. Since 2005, he has been with the Department of Electronic and Electrical Engineering, University of Sheffield, U.K., as a Lecturer and then as a Senior Lecturer. He has authored over 230 journal and conference papers, three book chapters, and a research monograph about wideband beamforming (Wideband Beamforming: Concepts and Techniques, Wiley, 2010).
His research interests are in sensor array signal processing, blind signal processing, multivariate signal processing and their various applications in wireless communications, radar, sonar, satellite navigation, human computer interface, and renewable energy exploitation.

Xianquan Wang received his B.S. degrees from TianJin University (State Key Lab of Precision Measuring Technology and Instruments) in 2015. He is currently working toward a Ph.D. degree in State Key Lab of Precision Measuring Technology and Instruments at TianJin University.
His research interest focuses on the underwater communication and detection.

Chunyue Li was born in HeBei, China, in 1993. She received the B.S. degree from Northeastern University, Shenyang, China in 2016. She is currently working toward the Ph.D. degree in TianJin University (State Key Lab of Precision Measuring Technology & Instruments), TianJin, China.
Her research interest focuses on the underwater acoustic detection and communication.

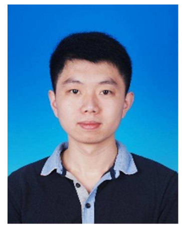

Lingran Bu was born in ShanDong, China, in 19994. He received his B.S. degrees from TianJin University (State Key Lab of Precision Measuring Technology and Instruments) in 2016. He is currently working toward a M.S. degree in State Key Lab of Precision Measuring Technology and Instruments at TianJin University.
His research interest focuses on the underwater acoustic signal detection, identification and classification.

Xiao Fu was born in ShanDong, China, in 1990. He received the B.Eng degrees from TianJin University, TianJin, China, in 2013. He is now a Ph.D. student at TianJin University (State Key Lab of Precision Measuring Technology & Instruments) since 2013.
His research interest focuses on the underwater communication and detection.

Tingting Huang was born in Hunan, China, in 1992. She received her Bachelor's degree from Tianjin University, Tianjin, China, in 2014. She is currently a doctor candidate in Tianjin University (State Key Lab of Precision Measuring Technology & Instruments).
Her research interest focuses on the underwater communication and detection.

Ling Ma was born in Shandong, China, in 1992. She received the B.E. degree from Tianjin University, and she is now pursuing her Ph.D. degree in the State Key Lab of Precision Measuring Technology & Instruments, Tianjin University, Tianjin, China.
Her research interest focuses on the underwater communication and detection.